

Large-Area Single-Crystal Graphene via Self-Organization at the Macroscale

Huy Quang Ta, Alicja Bachmatiuk, Rafael Gregorio Mendes, David J. Perello, Liang Zhao, Barbara Trzebicka, Thomas Gemming, Slava V. Rotkin,* and Mark H. Rummeli*

In 1665 Christiaan Huygens first noticed how two pendulums, regardless of their initial state, would synchronize. It is now known that the universe is full of complex self-organizing systems, from neural networks to correlated materials. Here, graphene flakes, nucleated over a polycrystalline graphene film, synchronize during growth so as to ultimately yield a common crystal orientation at the macroscale. Strain and diffusion gradients are argued as the probable causes for the long-range cross-talk between flakes and the formation of a single-grain graphene layer. The work demonstrates that graphene synthesis can be advanced to control the nucleated crystal shape, registry, and relative alignment between graphene crystals for large area, that is, a single-crystal bilayer, and (AB-stacked) few-layer graphene can be grown at the wafer scale.

The development of chemical vapor deposition (CVD) for synthetic single-crystalline graphene at the wafer-scale without grain boundaries between graphene domains, which, otherwise leads to the degradation of the graphene's electrical, thermal and mechanical properties, is vital. Thus far, two approaches have been exploited to obtain single-crystal graphene at the wafer-scale. The first strategy involves reducing the nucleation


density to grow a "giant" single domain of monolayer graphene. Such a process requires a complex substrate pretreatment which includes annealing at high temperature,^[1,2] polishing and oxidizing.^[3,4] The main drawbacks of this strategy are that the growth process usually requires a long reaction time and can be easily terminated by self-limited growth. The second strategy involves the unidirectional alignment of multiple graphene domains which coalesce to form a monocrystalline graphene layer over substrates which are either in a single-crystal phase or liquid phase. In the case of single-crystal substrates, hydrogen-terminated germanium (110),^[5] copper (111) surface^[6] and

hexagonal boron nitride (h-BN)^[7] have been demonstrated to work successfully. The underlying mechanisms are due to epitaxial growth on a low lattice mismatch substrate with that of graphene, for example, Cu (111) and h-BN, or, the presence of a step-pattern in Ge (110)^[8] which influence the co-alignment of the graphene domains during growth. Other examples of epitaxial growth are over Ni (111) by CVD^[9] and also by SiC

Dr. H. Q. Ta, Dr. R. G. Mendes, Dr. L. Zhao, Prof. M. H. Rummeli
Soochow Institute for Energy and Materials Innovations
College of Physics
Optoelectronics and Energy
Collaborative Innovation Center of Suzhou Nano Science
and Technology
Soochow University
Suzhou 215006, China

Dr. H. Q. Ta, Dr. R. G. Mendes, Dr. L. Zhao, Prof. M. H. Rummeli
Key Laboratory of Advanced Carbon Materials and Wearable Energy
Technologies of Jiangsu Province
Soochow University
Suzhou 215006, China

Dr. H. Q. Ta, Prof. A. Bachmatiuk, Dr. R. G. Mendes, Dr. T. Gemming,
Prof. M. H. Rummeli
Leibniz Institute for Solid State and Materials Research Dresden
P.O. Box 270116, Dresden D-01171, Germany
E-mail: m.ruemmeli@ifw-dresden.de

 The ORCID identification number(s) for the author(s) of this article can be found under <https://doi.org/10.1002/adma.202002755>.

© 2020 The Authors. Published by Wiley-VCH GmbH. This is an open access article under the terms of the Creative Commons Attribution License, which permits use, distribution and reproduction in any medium, provided the original work is properly cited.

DOI: 10.1002/adma.202002755

Prof. A. Bachmatiuk, Prof. B. Trzebicka Prof. M. H. Rummeli
Centre of Polymer and Carbon Materials
Polish Academy of Sciences
M. Curie-Skłodowskiej 34, Zabrze 41-819, Poland

Prof. A. Bachmatiuk
Polish Center for Technology Development (PORT)
Ul. Stabłowicka 147, Wrocław 54-066, Poland

Dr. D. J. Perello
School of Physics and Astronomy
The University of Manchester
Manchester M13 9PL, UK

Dr. D. J. Perello
National Graphene Institute
The University of Manchester
Booth St. E, Manchester M13 9PL, UK

Prof. S. V. Rotkin
Department of Engineering Science and Mechanics
Materials Research Institute
The Pennsylvania State University
Millennium Science Complex, University Park, PA 16802, USA
E-mail: vvr5@psu.edu

Prof. M. H. Rummeli
Institute of Environmental Technology
VSB-Technical University of Ostrava
17. Listopadu 15, Ostrava 708 33, Czech Republic

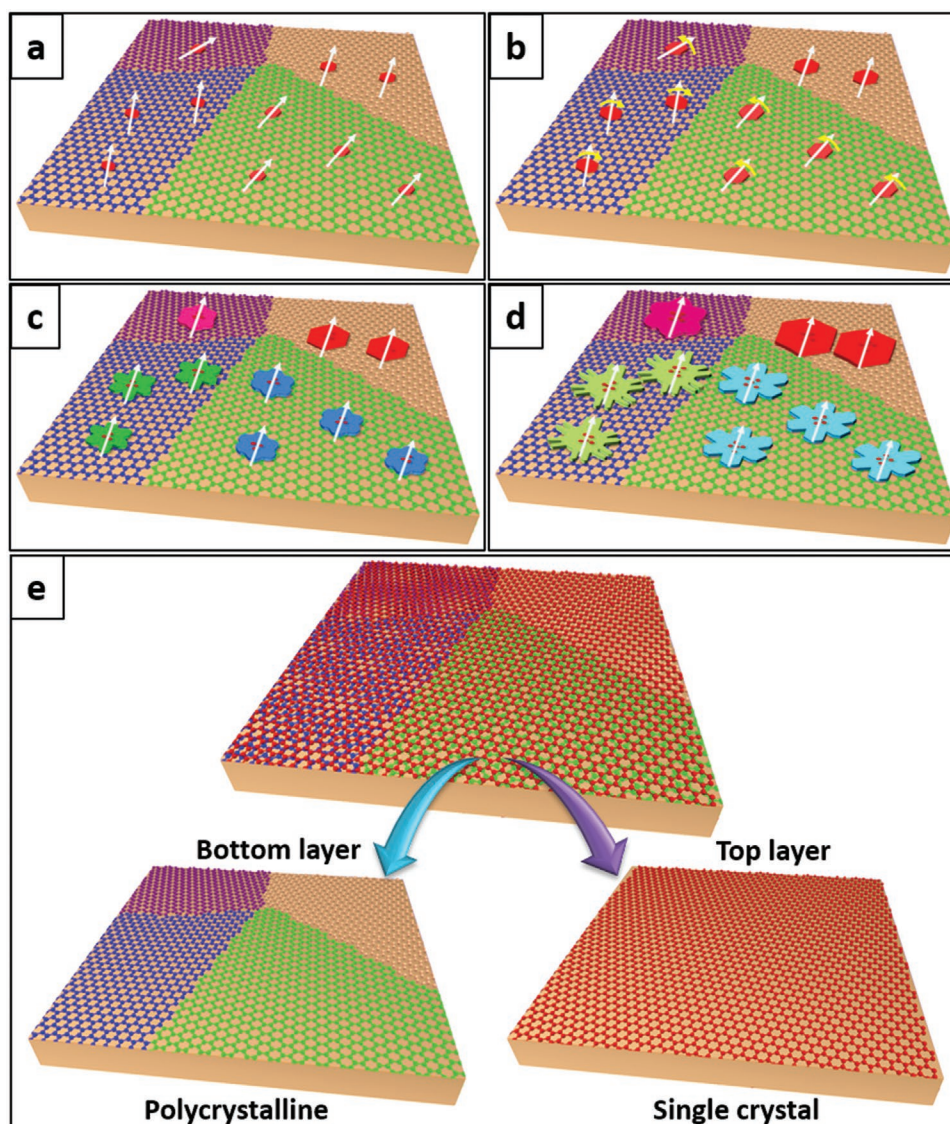


Figure 1. Schematics showing large-area single-crystal graphene growth steps from early grown secondary graphene flakes self-aligning over a polycrystalline graphene base. Secondary layer flakes all nucleate as randomly oriented AB-stacked hexagons initially (a). These flakes rotate (b) to form global self-alignment with respect to each other, overriding the underlying polycrystalline graphene orientations (c). As they grow larger these twisted flakes acquire more complex (fractal-like) shapes (c,d), which strongly correlates with the stacking rotation (twist) angle with respect to the underlying graphene. The self-aligned flakes merge as they grow to yield a large-area single-crystal graphene domain, namely, grain boundary free (e) on top of the polycrystalline graphene base.

sublimation.^[10] In an alternative method,^[11] when Cu is in a liquid phase (amorphous form), graphene domains form in an isotropic shape (circle) with mixed edges (sawtooth-like) which exhibit high activity. During coalescence, the orientation of adjacent grains can easily adjust to match each other when over a liquid Cu surface. The driving force is attributed to the energy minimization at the stitched region. Zeng et al.^[12] reported the self-assembly and alignment of graphene domains with a regular faceted shape (hexagon) over liquid metal surfaces.

In this work, we examine flakes forming over a contiguous polycrystalline graphene layer [Stranski–Krastanov (SK) growth] by chemical vapor deposition (CVD). We show the remarkable and ubiquitous self-alignment of secondary graphene domains after nucleation during SK growth over millimeter areas over

an initial base layer of polycrystalline graphene, namely, large-area single-crystal graphene forms over a polycrystalline substrate. The steps in which the early grown secondary graphene flakes self-organize at the macroscale enabling large-area single-crystal graphene to form are shown in **Figure 1**. Extensive statistical analysis shows that the nucleating secondary graphene domains always initially form as hexagons, presumably due to epitaxial considerations. The as-nucleated flakes initially adopt an AB (Bernal) stacking with the underlying graphene. Due to the random orientation of the primary layer domains, these flakes are also randomly aligned on the scale of a wafer. Yet, astonishingly, at a later stage of growth many flakes rotate to form a twisted bilayer configuration (which is a less favorable stacking configuration) in order to self-align globally,

and in doing so, the secondary domains continue growth, adopting a fractal-like shape. Thus, global alignment between secondary flakes dominates over the (non Bernal) stacking energy penalty, similar to that found with graphene growth over liquids in ref. [12]. Nucleation and formation of further layers above the self-aligned secondary domain automatically produce a new AB-stacked single-crystal lattice. Tertiary flakes already aligned at the nucleation stage, then merge to form a single-crystal AB-stacked tri- or few-layer graphene film.

The rotation of secondary flakes seems counterintuitive, yet the facts show that the flakes self-align their crystal orientations over the mm range and continue synchronized growth to ultimately form large-area single-crystal graphene (Movie S1, Supporting Information) without grain boundaries, as we now present.

Details of the SK growth of graphene are provided in the methods section and in more depth (for example aspects of the CH_4/H_2 ratio) in reference.^[13] Very briefly, to achieve SK growth, relatively high CH_4 to H_2 gas ratios are implemented in a chemical vapor deposition (CVD) process. The SK growth mode is a two-step process in which initially complete films of adsorbates form after which synthesis continues through nucleation and growth of adsorbate “islands” over the initially formed film. In this study, the SK growth of graphene is rapid and an initial full coverage of polycrystalline monolayer graphene forms over the Cu substrate in a matter of seconds. New secondary graphene flakes (islands) then nucleate above the fully grown initial graphene film.^[13] Moreover, we observe that the nucleation of AB-stacked secondary graphene domains occurs in a temporal pulsed (on/off) manner. Samples were prepared and collected for 3, 5 and 7 s with an average growth rate of the order of $0.5 \pm 0.1 \mu\text{m s}^{-1}$ (flake radius). Scanning electron microscopy (SEM) has been combined with Raman microscopy, dark-field transmission electron microscopy (DF-TEM), and selected-area electron diffraction (SAED) to unambiguously identify and correlate the twist and/or orientation angle and the shape of the flakes as well as to collect shape (reflecting twist angle) statistics for large number of flakes over a big surface area.

Electron backscatter diffraction (EBSD) studies confirmed the secondary flakes form above the initial graphene film.^[13] In short, previous studies have reported that for graphene growth over Cu(111) faces, the graphene always nucleates with a hexagonal shape. Moreover, the independent flakes are all oriented with respect to each other, so that when they merge, no grain boundary forms between the domains.^[6] This is due to the low lattice mismatch (4%) of graphene with the Cu (111) face which has strong influence on the growth. In the case of other Cu faces, the graphene domains are non-hexagonal.^[6] With this fact in mind we can carefully examine the flakes formed in our graphene (SK growth), such that if our bilayer flakes grew under the first layer and resided on a Cu(111) face, then they must be influenced by the Cu substrate leading to the formation of only hexagonal flakes. However, in this study, even on Cu (111) faces, we see a mix of hexagonal flakes and flower-like flakes. This tells us, that in our case, the bilayer flakes are not influenced by the Cu (111) surface and, thus, form on top of the surface of the initial graphene layer.^[13]

The SEM data showed that the flake edges exhibit various morphologies, however they all comprise a 6-fold symmetry

shape with six or twelve lobes. We found the morphology correlates with the bilayer twist angle, which allows for quantitative statistical analysis of flake orientations.^[14]

For all flakes, the 6-fold symmetry allows one to define a flake axes. Remarkably, **Figure 2-I** shows that these axes align over the entire substrate which is 5×5 mm, namely, crystal alignment occurs over the mm range. This is all the more astonishing given that the underlying monolayer graphene film is polycrystalline and randomly oriented (since the Cu support is also polycrystalline it should not help the alignment). **Figure 2-II** demonstrates reproducibility studies for a number of samples and shows that the orientation does not depend on the gas flow direction.

The lobe/corner alignment of the flakes occurs for well over 90% of all flakes. Alignment distortion at the macroscopic level can vary up to 7° which we attribute to distortions from the transfer process.

Although **Figure 2** provides an explicit visualization of the aligned growth phenomenon, defining a flake’s axial direction could be ambiguous for a flake with a complex shape and can be used for determining the global alignment only qualitatively. Thus, we combined SEM with transmission electron microscopy (TEM) studies to quantitatively confirm that the flakes align both in terms of lobe/axis orientation and crystal orientation, even though they grow over grains of different orientations in the underlying polycrystalline graphene film. **Figure 3-I** and **Figure S1**, Supporting Information, show relevant sections of the SEM images collected using TEM and then stitched together. Furthermore, DF-TEM confirms that the crystal alignment occurs in all flakes, across different grain boundaries with different stacking orientations (**Figures S1** and **S2**, Supporting Information). In depth analysis of the DF-TEM data show that the majority of the flakes are single crystalline (**Figure S5**, Supporting Information). With TEM we track the crystal orientations of the secondary flakes and the underlying polycrystalline graphene over the mm scale (**Figure 3-II** and **Figure S3**, Supporting Information). The reflexes from the Fourier domain, namely, SAED, provide the exact orientation angle. The data show a common crystal orientation for all flakes (**Figure 3**) over the mm scale despite a polycrystalline monolayer graphene substrate (**Figures S3** and **S4**, Supporting Information). The overall data (from SEM, DF-TEM, SAED and micro-Raman) confirm that the global crystal alignment of the flakes is independent of their registry with the underlying graphene. This is a key point and is one which we build on next.

To gain further insight into the alignment the relationship between the flake shapes and their stacking to the underlying graphene film was investigated. As shown in **Figure 4-I** and **Figures S6–S8**, Supporting Information, the most apparent correlation is that between the geometrical shape (faceting) of the flake (as seen in SEM or micro-Raman) and twist angle (from SAED and DF-TEM). Small twist angles are always observed in regular hexagonal flakes, while the complexity of the flake shapes increases and their perimeter becomes more fractal-like as the twist angle increases (**Figure 4-I**; **Figures S6–S8**, Supporting Information). As depicted in **Figure 1**, all secondary flakes nucleate with zero twist angle with respect to the graphene grain underneath, and are, thus, only aligned within a single grain domain. Upon global alignment, discussed later in

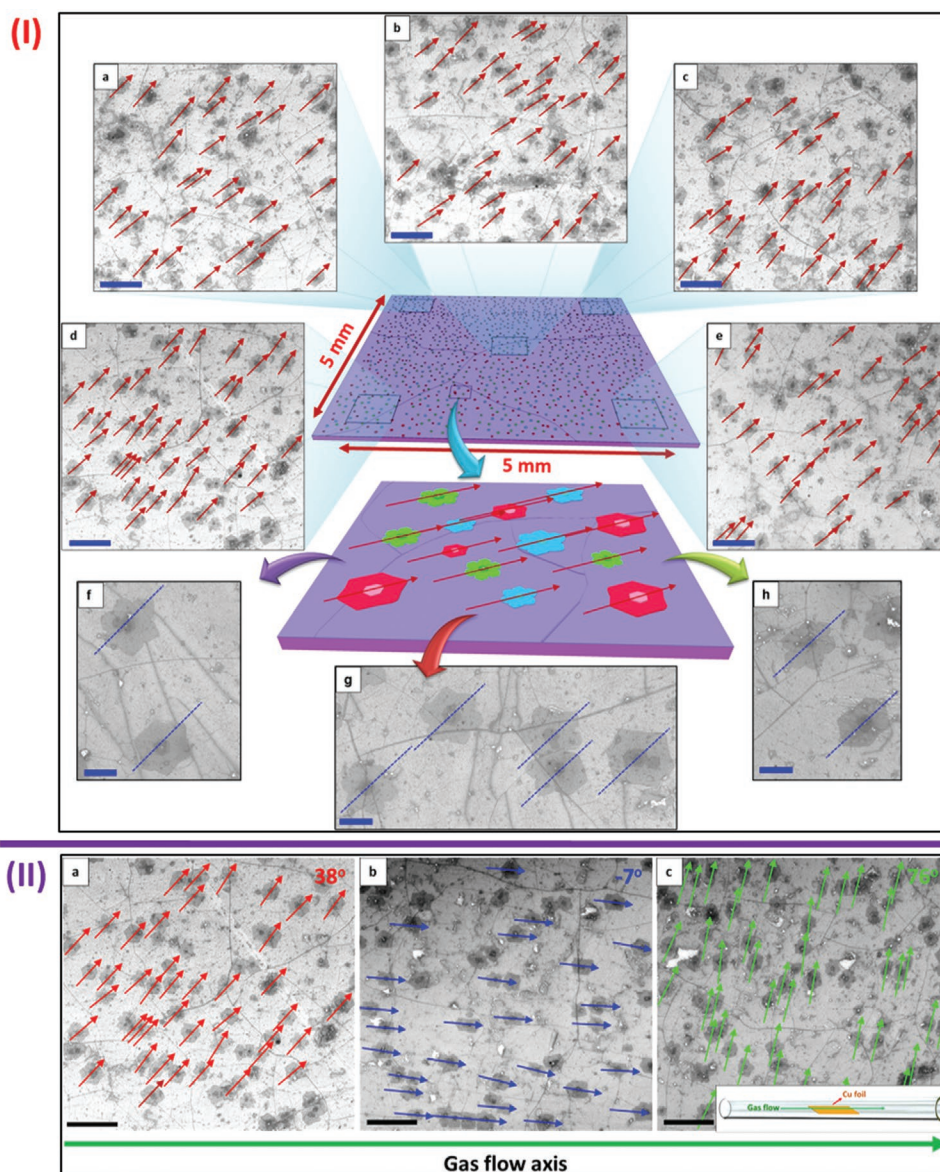


Figure 2. I) Example showing long range axes orientation of graphene crystals over large-scale (macroscopic) polycrystalline graphene (grown together by Stranski–Krastanov growth in CVD). a–e) SEM images taken in different positions from the same sample showing the long-range alignment of graphene flakes; scale bars = 10 μm . We observed that 93.6% of all the flakes are aligned with angle variation of $\approx 7^\circ$ at the macroscopic level. f–h) SEM images of flake alignment at higher magnification. Scale bars = 2 μm . II) Reproducibility of self-alignment: SEM images of different samples all demonstrating global alignment. No alignment with respect to the gas flow axis is observed (note: the gas axis is the same as the long axis of the CVD reactor tube). The inset in (c) shows the Cu foil placement within the reactor tube. All scale bars = 10 μm .

more detail, flakes acquire non-zero twist angle with respect to their parent grain, thus their further growth becomes diffusion limited and anisotropic, producing a dendritic edge for large twist angles.

Micro-Raman, while less accurate than the SAED technique to track flake orientation, does enable a larger number of flakes to be observed for superior correlation analysis (Figure S8, Supporting Information). Exploiting the dependence of the Raman G band ($\approx 1580\text{ cm}^{-1}$) and 2D band ($\approx 2670\text{ cm}^{-1}$) with respect to twist angle, one can broadly classify bilayer graphene into three different types; close to AB stacked with relative rotation angles of $0\text{--}5^\circ$ (A-type flakes), close to “critical angle”^[15] $7\text{--}14^\circ$ (B-type

flakes), and heavily twisted t-BLG, $17\text{--}30^\circ$ (C-type flakes).^[13,15,16] A statistical analysis of the different flake shapes and their relative stacking angle window from Raman spectroscopy is provided in Figure S6, Supporting Information, for samples with growth times of 3, 5 and 7 s.

Knowing the relationship between the shape and twist angle (see Figure 4-I), the SEM data allow one to study the kinetics of the process. For the shortest synthesis period of 3 s, only four flake shape categories can be identified: a pure hexagon shape occurs for a twist angle of 0° (Bernal graphene) which we label A*; and three structures that we label A1*, B*, and C*, with respect to their ever increasingly complex edge morphology;

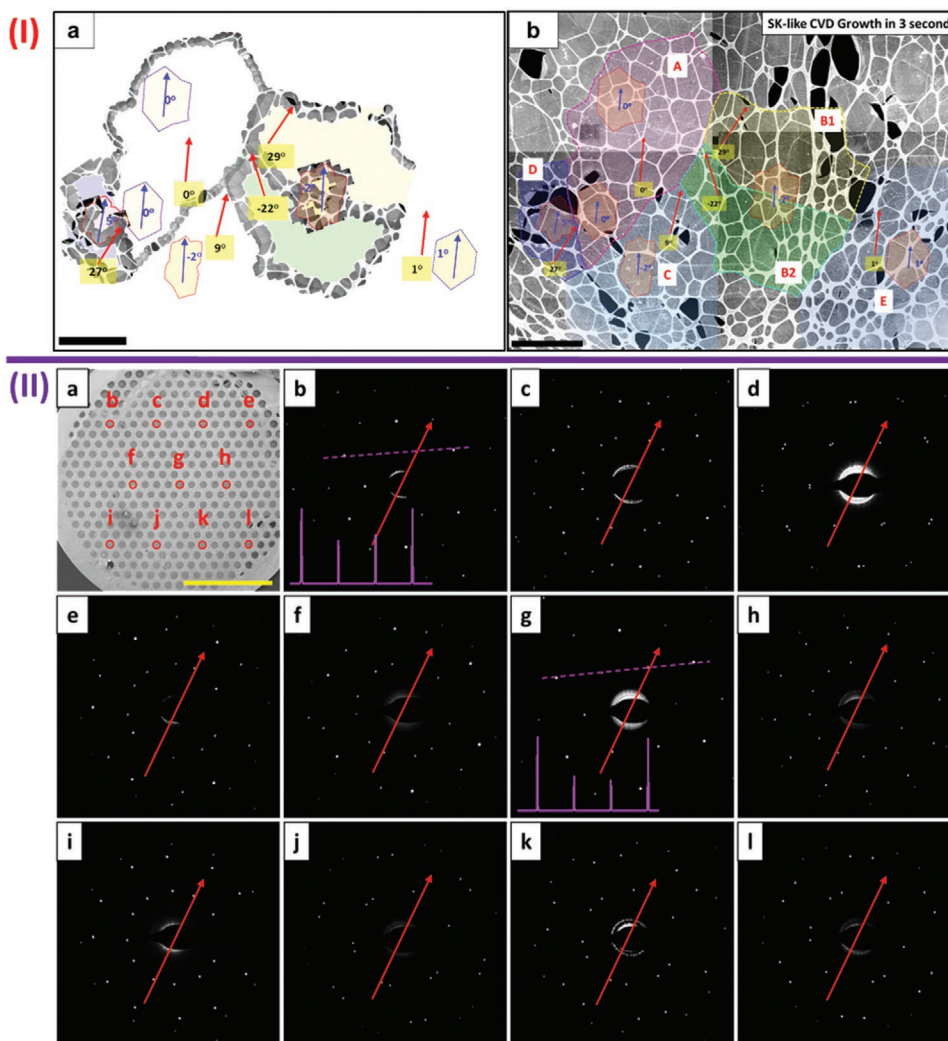


Figure 3. I) a,b) Grain mapping of graphene flakes over a poly-crystalline graphene film by DF-TEM (stitched together due to the limited field of view at higher magnifications in TEM). The data show that the graphene flakes are oriented/aligned independently of the crystal direction of the underlying graphene film. The red arrows with the numbers in the yellow boxes indicate the orientation of the underlying graphene film grains with respect to the orientation of grain A. The blue arrows with a blue number indicate the orientation of a given secondary flake with respect to the orientation of grain A. Scale bar is 5 μm . II) SAED data collected over the mm scale showing a common graphene domain orientation of bilayer flakes. SAED mapping over large area [millimeter scale as shown in (a)] showing that all the bilayer flakes have the same domain orientation (This is confirmed by comparing the data in Figure S3, Supporting Information, showing the base layer polycrystalline graphene grain orientations. Figure S4, Supporting Information, confirms the base layer is monolayer). Scale bar is 1 mm N.B. Small variations in the orientations can be seen ($\pm 2^\circ$), which we attribute to wrinkling due to the transfer process.

which correlate to increasing twist angle of 2–5°, 7–12°, and 17–28°, respectively. For the samples from longer CVD reaction times (5 and 7 s), six shape categories were identified: A, A1, B, B1, C, and C1, from a hexagonal shape at 0° to more complex fractal-like structures as the rotation angle increases. In particular, C1 and C have 12 clear lobes present. The data highlight that with increasing reaction time the partition is shifted towards twisted bilayer flakes. Visually, larger number of flakes evolve to have a more complex perimeter and this edge complexity (and lobe number) is greater for the larger twist angle between the flake and its primary (parent) grain. Despite the complexity of the flake shapes one can always determine their symmetry and orientation [Figure 4-II(a–c)], and, thus, define the global alignment axis

The statistical data also include cases when a particular flake is comprised two (or more, rarely) shapes/twist angles, easily observable from micro-Raman maps of the 2D to G mode intensity ratio. Examples from 3, 5, and 7 s samples are provided in Figure S8, Supporting Information, along with the SEM images of the same flakes. Such compound flakes should correspond to (occasional) close nuclei over two parent grains, merged together.

From the SEM (and micro-Raman) data we extract information on the growth rate of the flakes of different shapes/twist angles (Figure S9, Supporting Information): the average distance between flakes, the flake density, the average radius and the area of the flakes with respect to the CVD reaction time (3, 5, 7 s). The growth rate decreases with increasing reaction

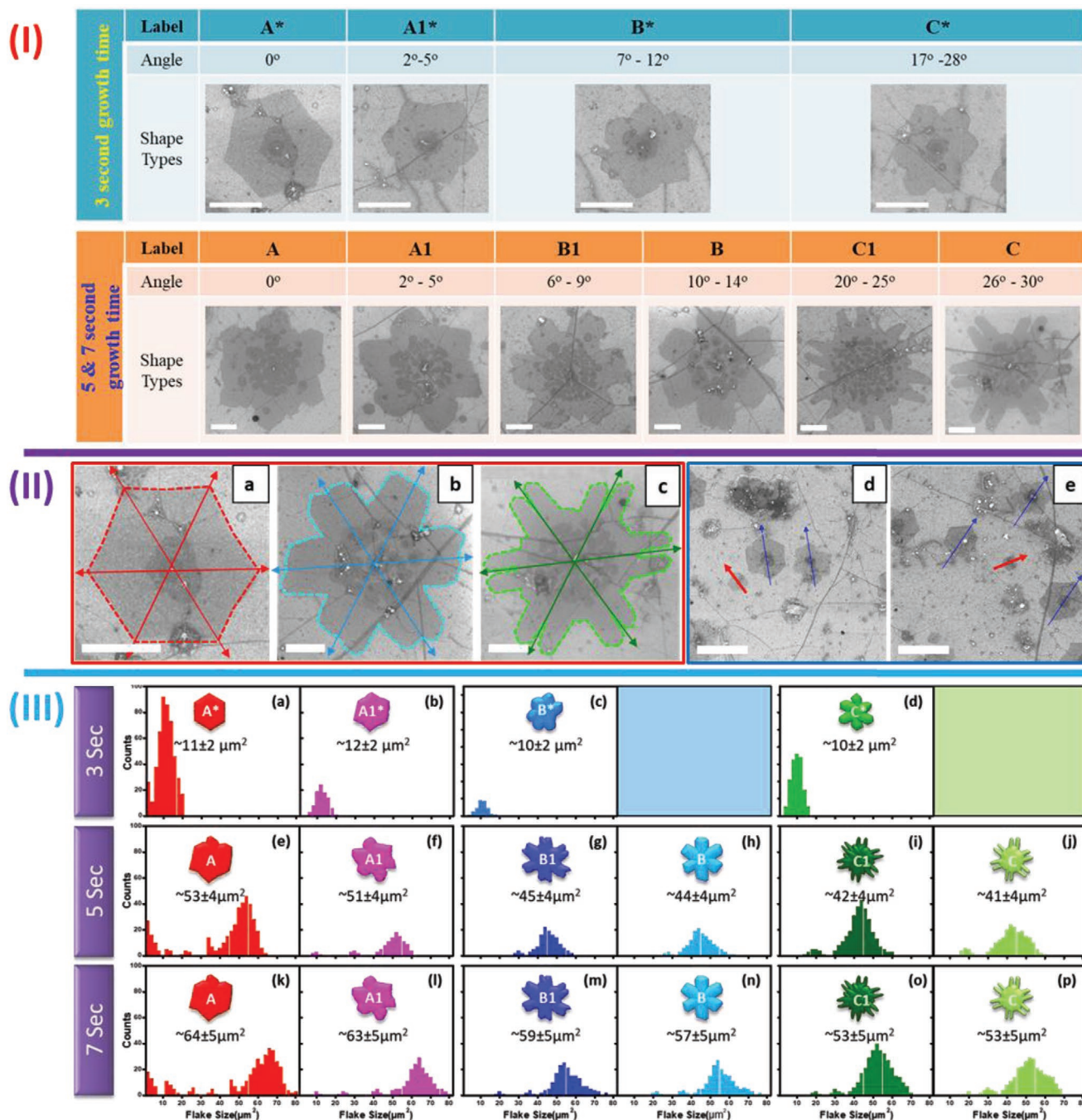


Figure 4. I) Flake shape correlation to its twist angle with respect to the underlying graphene. The top row shows the shape types (families) for flakes grown in 3 s. They are divided into four categories A*, A1*, B*, C* from low to high rotation angle. The bottom row shows the six shape (family) categories of flakes grown in 5 and 7 s. Note: Only four discernable categories are found for 3 s growth because after rotation the non-hexagonal flakes have had insufficient growth time to clearly present dendritic structures. All scale bars are 2 μm. II) Typical examples showing how one can determine the symmetry and orientation (axis) for different flake shapes for A type (a), B type (b), C type (c). d–e) SEM images showing examples of the non-aligned new-born hexagonal flakes prior to rotation [marked in red arrows against the dominant (global) alignment direction in blue arrows]. The scale bars in (a–c) are 2 μm and in (d–e) are 5 μm. III) Size/shape distribution of single-crystal graphene flakes (from SEM data) for different growth times. (a–d) show the distribution for the four shape categories after 3 s growth. (e–j) and (k–p) show the distribution for the six shape categories for flakes grown over 5 and 7 s growth, respectively. With longer growth times multiple peaks in growth distributions can be seen indicating pulsed or discrete nucleation. Only hexagons (shape type A) show a non-vanishing distribution at a very small size indicating all flakes nucleate as hexagons.

time which is reflected by a relative change in the rate of the average distance between flakes, radius and area (Figure S9c,d, Supporting Information). The growth rates depend on the flake

shape as follows: $A > B > C$, the more complex the flake shape, and hence the larger the perimeter, the slower the growth rate, which would support a diffusion-limited growth mechanism. The

flake density (Figure S9b, Supporting Information) increases with reaction time and this indicates that new nucleation of flakes takes place throughout the reaction. Moreover, nucleation of new flakes occurs in a temporal discrete manner. In Figure 4-III(a–p), we present the flake size distribution in terms of shape category (A, A1, B, B1, C, and C1), for the reaction growth times larger than 3 s multiple peaks are seen in the distribution function. Although smaller than the main peak, coming from initial nucleation, these peaks are distinct and follow the same growth rates as the majority of flakes [Figure S9d (inset), Supporting Information].

The size distribution data [Figure 4-III(a–p)] show that only shapes of type A, namely, hexagons exist close to zero which indicates that all flakes initially nucleate as hexagons (Bernal stacking with respect to the under layer) and therefore a single rotation to form a twisted bilayer configuration occurs post nucleation.

Since the data in Figure 4-III(a–p) suggests all flakes nucleate as AB-stacked hexagons and we know the bottom layer is polycrystalline with random grain crystallographic directions, then we should be able to find small hexagon flakes that follow the parent grain orientation and are not aligned with the majority of those that nucleated earlier and have already synchronized their orientation to the global axis; we observe small hexagonal flakes not aligned with the global flake alignment axis. Such flakes are shown in Figure 4-II(d,e) and Figure S10, Supporting information. Moreover, these newly nucleated hexagon flakes are AB stacked as confirmed in Figure S11, Supporting Information. This indicates that growing hexagons rotate *after* nucleation to align with a single (global) flake alignment direction. The size of the hexagonal flakes not aligned to the global orientation are less than 1–3 μm in diameter. One can safely assume that the upper size limit for rotation is close to this value as, in general, we do not see larger misaligned flakes. We attribute this to the thermally activated rotations becoming frustrated as the flake sizes increases due to the increased rotational friction. The flakes become aligned along the global axis, leading to a twisted registry with the supporting grain, with the twist angle depending on the grain lattice orientation. The twist angle determines the anisotropy of further growth, during the post rotation stage, and the edge shape as explained below.

A more comprehensive statistical evaluation of the different flake shapes (Figure S12, Supporting Information) shows that the most common shape for single-crystal flakes is the hexagon (A/A1) followed by C1/C2 which is close to 30° twist. The same pattern is also true for the flakes of mixed shape, and in keeping with the above, flakes combining A/A1 and C/C1 shapes dominate. This is consistent with polycrystalline support layer having grains of two major orientations at $\approx 30^\circ$ to each other. Interestingly, the second energetically preferred twist registry from CVD grown graphene tend to have twist angles between 20° and 30° ,^[17] which matches our statistics of C-type flakes.

The dominance of the A type shape means that, while the major contribution to the free energy is due to the global alignment of the flakes, the overall global axis is along the dominant orientation of the grains in the polycrystalline substrate. Indeed, the AB-stacked bilayer graphene configuration is energetically and kinetically preferred (cf. all flakes nucleate as hexagons). One can consider this to be the equilibrium graphene

shape under our CVD conditions, commensurate with the underlying graphene film. Upon rotation though, the registry between the flake and underlying film is altered, increasing the external chemical potential, μ_{ext} , (the internal chemical potential, μ_{int} , remains constant). An increase in the total chemical potential, $\mu = \mu_{\text{int}} + \mu_{\text{ext}}$ may lead to finger formation (fractal-like structure) on a growing flake by changing the growth kinetics toward a slower rate.^[18–21] The actual value of μ will depend on the relative orientation and anisotropy of the surfaces. Moreover, the larger perimeter of increasingly fractal-like structures will lead to even slower growth, as compared to hexagons and less fractal-like shapes, in agreement with our experimental observations.

As mentioned above, nucleation and initial growth lead to formation of hexagons with AB stacking with respect to parent graphene grains (confirmed by the micro-Raman, SAED and DF-TEM). Orientations of such hexagons would be consistent over a single grain domain and randomly distributed on a large scale. Since large size flakes, in addition to hexagons also show fractal-like shapes (with non-zero twist angle), and all flakes have the same orientation, the only possible explanation is that some hexagon flakes rotate in the early stages of growth into a twisted-angle globally aligned configuration, and then adopt a fractal-like shape (with lobes) because of the anisotropic growth conditions. The SAED and DF-TEM data provide the actual crystal orientation of both the secondary flakes after rotation and that of the graphene substrate, globally. The data show a full synchronization of all flakes across the mm range. We speculate that this synchronized growth is the reason for the re-orientation of small flakes. We assume these flakes experience thermal orientation fluctuations around a preferred global axis until frozen at a given size when the thermal energy drops below the rotational friction threshold. The all-synchronized flakes grow, depending on local twist registry, either still in hexagonal shape (most favorable configuration), or in fractal shape, until they start to merge in to a complete second layer.

In **Figure 5**, a group of at least three secondary flakes merge over three independent primary grains with different orientations from the base graphene. The data show the merged flakes form a large single-crystal piece of graphene without grain boundaries. This large single-crystal secondary grain lies across three different primary grain orientations of the base polycrystalline graphene. Hence, for longer growth periods these flakes would merge with other synchronized flakes to form a single-crystal (secondary) graphene layer over the whole sample (as confirmed in **Figure 6** and in section B with Figures S13 to S23, Supporting Information). Moreover, new flakes forming over secondary large-area single-crystal graphene (in turn formed over the polycrystalline base layer) will all have the same (Bernal) orientation when as-nucleated. The DF-TEM (as shown in Figure 5e) shows that tertiary hexagon crystals are fully aligned. This demonstrates that the technique, aside from yielding large-area single-crystalline graphene, can also yield large area AB-stacked bi-, tri-, and multi-layer Bernal graphene.

From this remarkable synchronization process the key question remains; what is/are the driving force/s to rotate the secondary layer flakes that aligns their lobes and more importantly, aligns them to a single common crystal orientation over very large ranges? At this stage it is not obvious what the

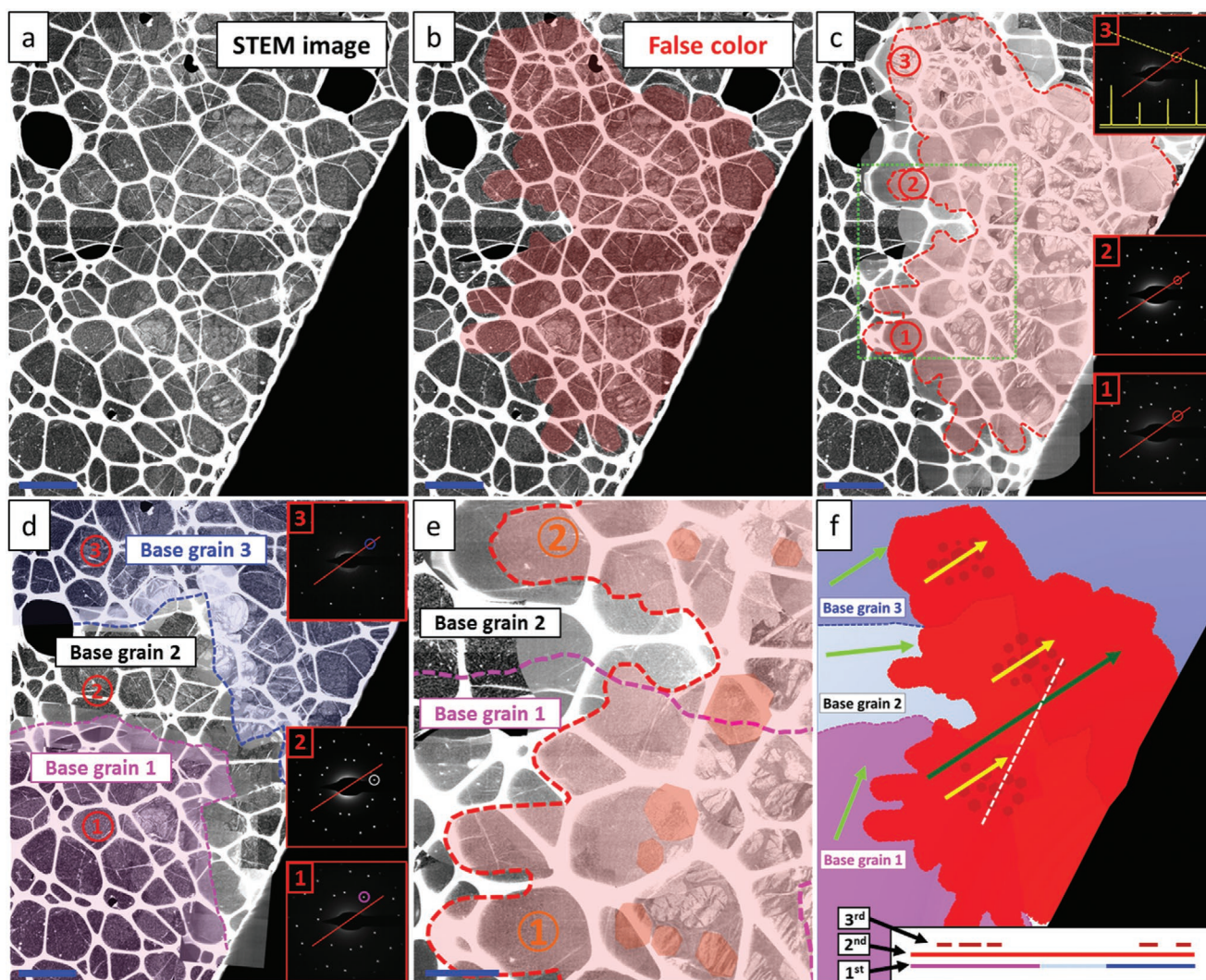


Figure 5. Typical example of common alignment of secondary (and ternary) flakes over a polycrystalline graphene substrate. a) Stitched scanning transmission electron microscopy (STEM) image of SK-bilayer graphene transferred on to a lacey carbon TEM grid. Changes in contrast reveal bi- and trilayers over the underlying base graphene. b) STEM image with false color to highlight bilayer regions. c) Stitched DF-TEM images overlapping the STEM image confirm that the merged bilayer graphene piece is a single crystal, and trilayer graphene flakes above are AB-stacked with respect to the single (bilayer) piece below. Labels 1, 2, and 3 represent SAED measurement (aperture) regions (red circles highlighted in the image). The red lines in the SAED inset represent the common crystal orientation of the bilayer graphene. The red circles in the SAED insets indicate the position of the objective aperture for DF-TEM mapping. d) Stitched DF-TEM images overlapping a STEM image confirming the polycrystallinity of underlying graphene. The single-crystal bilayer graphene from various merged flakes) cross over three grains from the underlying base graphene. The pink, white, and blue circles in SAED highlight the crystal orientation of underlying graphene grains 1, 2, and 3, respectively. e) Magnified image of stitched DF-TEM from green dashed box in (c) for detailed observation of the single-crystal bilayer graphene crossing over various grains from the underlying graphene. f) A simple schematic to describe the structure of layers and their crystal orientation (one color corresponds to one crystal orientation). The green, dark green, and yellow arrows indicate the crystal orientation of the first, second and third layer, respectively. Inset shows the cross-section from the white dashed line. Scale bars are 2 μm for (a–d) and 1 μm for (f).

underlying mechanism is, however, we can postulate some ideas. We begin with mechanisms we can rule out, namely, the formation of a macroscopic electrostatic field to align the flakes, since our polycrystalline Cu foil over which the graphene film and subsequent flakes form is conductive and so would screen an electrostatic potential at a distance of around one nanometer. Alignment due to macroscopic gas flow can also be ruled out since our studies show there is no correlation of the alignment axis and the gas flow direction. In addition, anisotropy in adatom diffusion constants due to the crystal orientation of

underlying graphene must be neglected since the polycrystalline graphene film does not have a single orientation and, in addition, this would contradict our observation of the alignment process occurring at a global level, even across grain boundaries. One possible mechanism could rely on an adatom diffusion gradient which could arise along the dominant orientation (in terms of cumulative surface flake area) of the initially formed hexagonal flakes (base shape A). This direction might be then related to the dominant grain orientation of the first layer graphene film (and ultimately the dominant grains of the

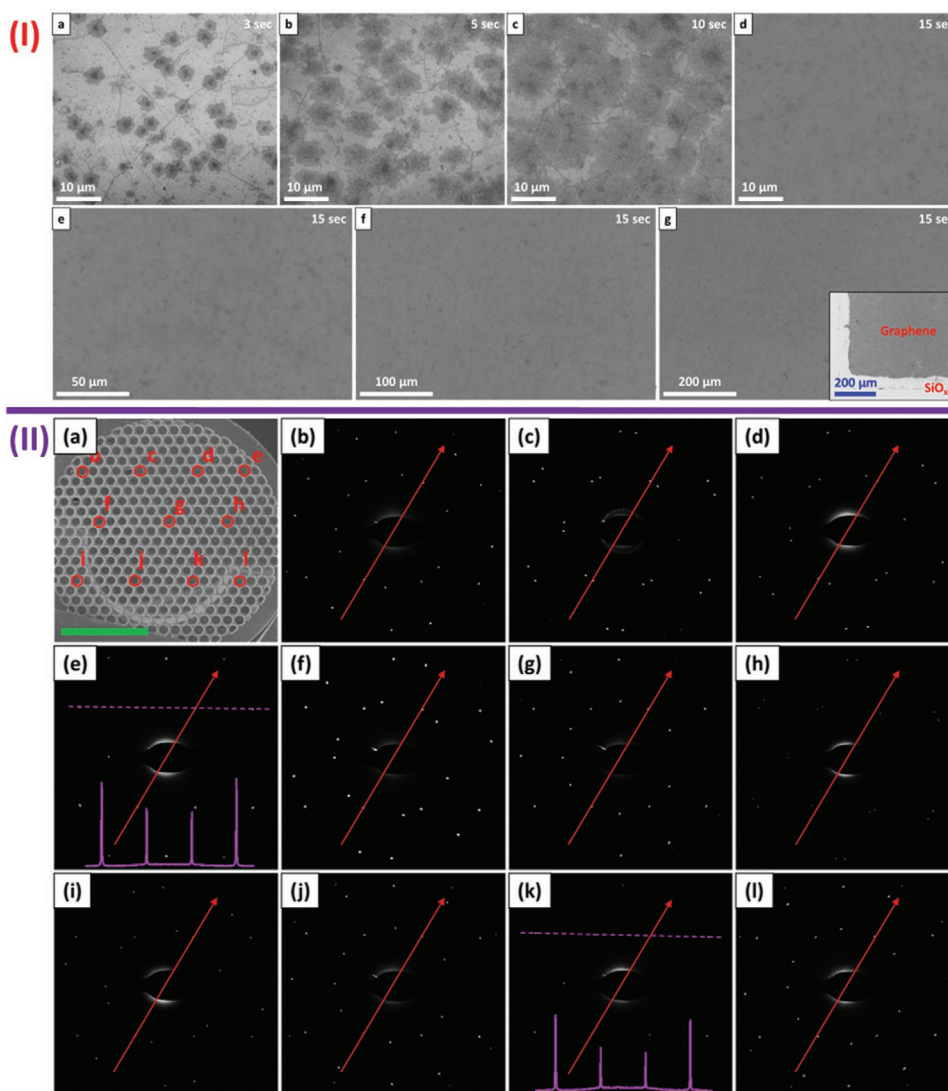


Figure 6. I) Time evolution of bilayer graphene growth. a–d) SEM images showing time dependent growth of bilayer graphene from small islands at 3 s (a) to full coverage at 15 s (d). e–g) SEM images at lower magnification of the 15 s growth time. II) SAED data collected over the mm scale from full coverage bilayer graphene (15 s growth time) showing a common graphene domain orientation of bilayer graphene. SAED mapping over large area [millimeter scale as shown in (a)] showing that all the measured bilayer areas have the same domain orientation (b–l). For (e) and (k) the intensity profiles over the [1010] and outer [1120] reflexes are presented as the graphene is AB stacked in these regions. The larger intensity of the outer [1120] reflexes confirms bi-layer graphene. Scale bar is 1 mm.

Cu substrate), namely, epitaxial aspects between the underlying graphene and the bilayer flakes dictate the prevailing diffusion gradient direction that defines the global axis. Should the flakes have strong and anisotropic interactions, the synchronization could emerge spontaneously, as an order parameter in phase transitions—which is an intriguing possibility. We note that the flake statistics indicate that the nucleation and/or growth are discrete (pulsed in time). Therefore, it could be that during periods of intense growth the adatom concentration (and flux) fields are much larger and fluctuate strongly (non-uniform), thus producing substantial synchronization over macroscopic areas. Additionally, the nucleation of tertiary flakes above the main flakes (which are experimentally observed, e.g., Figure 2) may disturb the growth. Indeed, before a tertiary flake is formed, the whole top surface of secondary flake may collect

the carbon stock from the gas phase and contribute to flake growth, along with the open area outside the flake. The ratio of the (local) flux of add-atoms from flake surface (flake flux) to the external (primary) flux on the underlying graphene substrate increase with growth time, until the tertiary flake nucleates. The local flux contribution from the flake surface could overcome and destroy the global lobe alignment synchronization derived from the primary flux of C species on the graphene substrate outside the flake. Once the third layer nucleates, the surface flux would not contribute much to secondary flake growth, rather being consumed by the tertiary flake. Then the flux of primary flakes returns to a stage similar to that found before, right after the secondary flake formation and thus the creation of the global alignment order derived from local inter-flake interactions would continue. In this way, the nucleation of

new secondary flakes would also occur in a discrete manner (as observed). In short, variations in the partial fluxes could account for both the synchronized alignment and pulsed nucleation of new flakes. Strain may also play a role in the synchronization process. Strain from the underlying graphene could lead to a diffusion gradient or anisotropic concentration of adatoms. It is well known that graphene in seeking to be as commensurate as possible with the underlying substrate (copper in our case) will stretch or compress depending on the underlying crystal structure. Of course, in this work the underlying Cu is polycrystalline and so the local strain varies depending on the underlying Cu grain orientation, however, that said, one could envisage a net strain forming globally on the graphene film which in turn alters the commensurability of the graphene flakes growing over its surface. This process would depend on the size of the flake such that for very small flakes the influence of strain is limited and commensurability will be closer to that of AB stacking with the underlying graphene. As the flake grows, the effect of lattice distortions in the underlying graphene film will be more pronounced as the interaction area is larger such that eventually a growing flake instantly rotates to release the stress. We cannot exclude that the flake-to-flake interactions can be facilitated by thermal phonons (at high synthesis temperature) or, given, both the Cu and graphene substrate are conductive, by plasmons (with or without charge exchange). It may also be true that both strain, potential and diffusion gradients play a role simultaneously enabling the long-range cross-talk (synchronized alignment) between flakes which is experimentally observed.

In summary, we have shown that CVD-grown graphene crystals forming over a graphene substrate during Stranski–Krastranov growth always nucleate as hexagons and in the lowest energy stacking configuration, namely, Bernal stacking. However, most of these new (secondary) crystals have a tendency to rotate and adopt a common crystal alignment after nucleation and initial growth. Since the initial polycrystalline graphene has grains of multiple orientations, a sub-population of secondary flakes becomes non-AB-stacked (twisted). Subsequently, some of the secondary crystals adopt a fractal-like shape since the surface potential between the graphene film and crystal increases upon misorientation. The complexity of the fractal-like shape thus correlates with the stacking twist angle between the flake and the underlying graphene. Remarkably all the graphene crystal flakes align their lobe and crystal orientation globally over the mm scale regardless of their shape or twist angle/registry with the underlying polycrystalline graphene. We conclusively show how this synchronization process allows for large area single-crystal graphene formation over a polycrystalline base/substrate. Moreover, subsequent layer formation yields AB-stacked graphene. The synchronization process of the secondary graphene flakes, we hypothesize, is due to (global) strain and/or fluctuation potential and/or diffusion gradients. The observations shown in this work provide astonishing insight into graphene formation and demonstrate global cross-talk between growing graphene crystals is possible and could pave the way for advanced synthetic graphene (and other 2D materials) procedures in terms of crystal shape, registry and relative alignments between graphene crystals at the macro-scale and large-area single-crystal 2D material fabrication.

Experimental Section

CVD Growth: Stranski–Krastranov-like graphene was synthesized using an atmospheric pressure CVD system over polished copper with methane (99.999%) as the feedstock. In the CVD system, the reaction takes place in a horizontal quartz tube of length 75 cm and diameter of 5 cm. In order to obtain a flat substrate, a 100 μm thick copper foil (from Nilaco, 99.96%) was pre-annealed at 1060 $^{\circ}\text{C}$ with 1000 sccm Ar and 200 sccm H_2 for 2 h, then polished using a chemical mechanical polishing method.^[13] The polished copper was then loaded in the chamber and heated up to 1060 $^{\circ}\text{C}$ in 40 min with constant flow of 1000 sccm Ar and 200 sccm H_2 . After reaching 1060 $^{\circ}\text{C}$, the copper foil was annealed for 1 h with the same gas flow. During the growth process, H_2 was reduced to 70 sccm and CH_4 was set at 30 sccm while Ar was maintained at 1000 sccm. For the CVD growth of SK-like graphene, reactions times of 3, 5 and 7 s were applied (the growth time was controlled by measuring time between switching on and off the CH_4 and H_2 mass flow controllers. After the reaction, the CH_4 and H_2 flows were shut down and the sample was cooled to room temperature in Ar and then removed.

Graphene Transfer: After growth, a poly(methyl methacrylate) (PMMA) solution (950 k C4), was spin-coated on the graphene/Cu at 1000 rpm for 60 s to protect the graphene film during transfer process. The sample was floated in copper etchant (CE-100, Transene) for ≈ 30 min to etch the Cu substrate. The PMMA/graphene layer was rinsed thoroughly in deionized water several times and then transferred onto an SiO_2 (300 nm)/Si wafer. After drying in an oven (80 $^{\circ}\text{C}$ in 10 min), the sample was dipped in acetone for 2 min to remove the PMMA. For TEM characterization, the same process was also used for a transfer onto a lacy carbon grid.

Characterization: A confocal Raman CRM 200 (Witec, Germany) with 100 \times lens (Olympus, N.A. 0.9) and ≈ 1 mW power from 532 nm excitation laser was implemented for Raman spectroscopy and mapping. For SEM characterization, a field emission scanning microscope JSM-7600F (JOEL, Korea) at 15 kV was used. A FEI Titan cubed image Cs corrected TEM with an acceleration voltage of 80 kV was used for TEM image, DF-TEM image, and electron diffraction patterns acquisition.

Supporting Information

Supporting Information is available from the Wiley Online Library or from the author.

Acknowledgements

This work was supported by the National Science Foundation China (NSFC, Project 51672181), the Czech Republic from ERDF “Institute of Environmental Technology – Excellent Research” (No. CZ.02.1.01/0.0/0.0/16_019/0000853). M.H.R. thanks the Sino-German Research Institute for the support (Project: GZ 1400). S.V.R. acknowledges NSF (ECCS-1509786). H.Q.T. is grateful for the financial support of an Alexander von Humboldt Foundation Fellowship. The authors are grateful to Young Hee Lee for useful discussions.

Open access funding enabled and organized by Projekt DEAL.

Conflict of Interest

The authors declare no conflict of interest.

Author Contributions

M.H.R. and S.V.R. conceived the experiments and developed the analytical framework. M.H.R. supervised the work. H.Q.T. conducted the synthesis experiments. Characterizations were conducted by H.Q.T.

A.B., R.G.M., and D.J.P. All authors contributed to the analysis of the work and the preparation of the manuscript.

Keywords

2D materials, bilayer graphene, global alignment, graphene, stacking order

Received: April 23, 2020

Revised: July 11, 2020

Published online: September 23, 2020

-
- [1] Z. Yan, J. Lin, Z. Peng, Z. Sun, Y. Zhu, L. Li, C. Xiang, E. L. Samuel, C. Kittrell, J. M. Tour, *ACS Nano* **2012**, *6*, 9110.
- [2] L. Gao, W. Ren, H. Xu, L. Jin, Z. Wang, T. Ma, L.-P. Ma, Z. Zhang, Q. Fu, L.-M. Peng, X. Bao, H.-M. Cheng, *Nat. Commun.* **2012**, *3*, 699.
- [3] G. H. Han, F. Güneş, J. J. Bae, E. S. Kim, S. J. Chae, H.-J. Shin, J.-Y. Choi, D. Pribat, Y. H. Lee, *Nano Lett.* **2011**, *11*, 4144.
- [4] Y. Hao, M. S. Bharathi, L. Wang, Y. Liu, H. Chen, S. Nie, X. Wang, H. Chou, C. Tan, B. Fallahazad, H. Ramanarayan, C. W. Magnuson, E. Tutuc, B. I. Yakobson, K. F. McCarty, Y.-W. Zhang, P. Kim, J. Hone, L. Colombo, R. S. Ruoff, *Science* **2013**, *342*, 720.
- [5] J.-H. Lee, E. K. Lee, W.-J. Joo, Y. Jang, B.-S. Kim, J. Y. Lim, S.-H. Choi, S. J. Ahn, J. R. Ahn, M.-H. Park, C.-W. Yang, B. L. Choi, S.-W. Hwang, D. Whang, *Science* **2014**, *344*, 286.
- [6] V. L. Nguyen, B. G. Shin, D. L. Duong, S. T. Kim, D. Perello, Y. J. Lim, Q. H. Yuan, F. Ding, H. Y. Jeong, H. S. Shin, S. M. Lee, S. H. Chae, Q. A. Vu, S. H. Lee, Y. H. Lee, *Adv. Mater.* **2015**, *27*, 1376.
- [7] W. Yang, G. Chen, Z. Shi, C.-C. Liu, L. Zhang, G. Xie, M. Cheng, D. Wang, R. Yang, D. Shi, K. Watanabe, T. Taniguchi, Y. Yao, Y. Zhang, G. Zhang, *Nat. Mater.* **2013**, *12*, 792.
- [8] J. Dai, D. Wang, M. Zhang, T. Niu, A. Li, M. Ye, S. Qiao, G. Ding, X. Xie, Y. Wang, P. K. Chu, Q. Yuan, Z. Di, X. Wang, F. Ding, B. I. Yakobson, *Nano Lett.* **2016**, *16*, 3160.
- [9] Y. Yang, Q. Fu, W. Wei, X. Bao, *Sci. Bull.* **2016**, *61*, 1536.
- [10] N. Mishra, J. Boeckl, N. Motta, F. Iacopi, *Phys. Status Solidi A* **2016**, *213*, 2277.
- [11] M. Zeng, L. Tan, L. Wang, R. G. Mendes, Z. Qin, Y. Huang, T. Zhang, L. Fang, Y. Zhang, S. Yue, M. H. Rummeli, L. Peng, Z. Liu, S. Chen, L. Fu, *ACS Nano* **2016**, *10*, 7189.
- [12] M. Zeng, L. Wang, J. Liu, T. Zhang, H. Xue, Y. Xiao, Z. Qin, L. Fu, *J. Am. Chem. Soc.* **2016**, *138*, 7812.
- [13] H. Q. Ta, D. J. Perello, D. L. Duong, G. H. Han, S. Gorantla, V. L. Nguyen, A. Bachmatiuk, S. V. Rotkin, Y. H. Lee, M. H. Rummeli, *Nano Lett.* **2016**, *16*, 6403.
- [14] In brief, extensive data from combined SEM, micro-Raman, DF-TEM and SAED allow one to unambiguously identify and correlate the twist angle and the shape of the flakes. After this, SEM shape analysis was performed to collect twist angle statistics for a large number of flakes over a big surface area.
- [15] K. Kim, S. Coh, L. Z. Tan, W. Regan, J. M. Yuk, E. Chatterjee, M. F. Crommie, M. L. Cohen, S. G. Louie, A. Zettl, *Phys. Rev. Lett.* **2012**, *108*, 246103.
- [16] R. W. Havener, H. Zhuang, L. Brown, R. G. Hennig, J. Park, *Nano Lett.* **2012**, *12*, 3162.
- [17] L. Brown, R. Hovden, P. Huang, M. Wojcik, D. A. Muller, J. Park, *Nano Lett.* **2012**, *12*, 1609.
- [18] Z. Zhang, Y. Liu, Y. Yang, B. I. Yakobson, *Nano Lett.* **2016**, *16*, 1398.
- [19] T. Ma, W. Ren, X. Zhang, Z. Liu, Y. Gao, L.-C. Yin, X.-L. Ma, F. Ding, H.-M. Cheng, *Proc. Natl. Acad. Sci. USA* **2013**, *110*, 20386.
- [20] P. C. Rogge, K. Thürmer, M. E. Foster, K. F. McCarty, O. D. Dubon, N. C. Bartelt, *Nat. Commun.* **2015**, *6*, 6880.
- [21] V. I. Artyukhov, Y. Liu, B. I. Yakobson, *Proc. Natl. Acad. Sci. USA* **2012**, *109*, 15136.